Experimental investigations and thermodynamic modelling of the ternary system Pb-Mo-O

van Hattem, Andries; Dankelman, Robert; Colineau, Eric; Griveau, Jean-Christophe; Dardenne, Kathy; Rothe, Jörg; Couweleers, Sebastian; Konings, Rudy J.M.; Smith, Anna L.

DOI
10.1016/j.jallcom.2024.175588

Publication date
2024

Document Version
Final published version

Published in
Journal of Alloys and Compounds

Journal of Alloys and Compounds 1003 (2024) 175588

Contents lists available at ScienceDirect

Journal of Alloys and Compounds

journal homepage: www.elsevier.com/locate/jalcom

Experimental investigations and thermodynamic modelling of the ternary system Pb-Mo-O

Andries van Hattem [a], Robert Dankelman [a], Eric Colineau [b], Jean-Christophe Griveau [b], Kathy Dardenne [c], Jörg Rothe [c], Sebastian Couweleers [a], Rudy J.M. Konings [a], Anna L. Smith [a,*]

[a] Faculty of Applied Sciences, Radiation Science & Technology Department, Delft University of Technology, Mekelweg 15, Delft 2629JB, the Netherlands
[b] European Commission, Joint Research Centre, P.O. Box 2340, Karlsruhe D-76125, Germany
[c] Karlsruhe Institute of Technology (KIT), Institute for Nuclear Waste Disposal (INE), Radionuclide Speciation Department, Hermann-von-Helmholtz-Platz 1, Eggenstein-Leopoldshafen 76344, Germany

ARTICLE INFO

Keywords:
Pb-Mo-O
CALPHAD
Thermodynamic modelling
Molybdates
Lead-cooled Fast Reactor
X-ray Diffraction
XANES
2000 MSC:
0000
1111
PACS:
0000
1111

ABSTRACT

A combined experimental and modelling study into the Pb-Mo-O system has been conducted in view of the safety analysis for lead-cooled nuclear systems. The thermal expansion and low-temperature heat capacity of the ternary compounds $PbMoO_4$ and Pb_2MoO_5 have been determined experimentally, as well as the melting enthalpy of $PbMoO_4$. Moreover, XANES measurements have confirmed the hexavalent oxidation state of Mo in $PbMoO_4$ and Pb_2MoO_5.

A thermodynamic model of the ternary system including the ternary phases $PbMoO_4$, Pb_2MoO_5 and Pb_5MoO_8 has also been developed in this work based on the CALPHAD methodology. For the first time, an ionic two-sublattice model is used for the liquid phase, while the compound energy formalism is used for the solid phases.

1. Introduction

Although the ternary system Pb-Mo-O has been the subject of many investigations, driven both by fundamental interests and diverse technological applications, some fundamental properties of these materials have never been experimentally studied and a recent thermodynamic model is lacking in literature. Lead molybdate $PbMoO_4$ has been investigated for scintillation [1], luminescence [2–5] and acousto-optical applications [6], and already in 1921, a phase diagram of the PbO-$PbMoO_4$ section has been published by Jaeger and Germs [7].

Recently, the Pb-Mo-O system has received renewed attention in the field of nuclear engineering, in the framework of safety assessment of the Lead-cooled Fast Reactor (LFR), a nuclear reactor cooled with liquid Pb or a liquid lead-bismuth eutectic mixture (LBE) [8,9]. The use of this coolant was first applied in Soviet submarines [10–12]; nowadays, Pb and LBE are coolant candidates for Accelerator Driven Systems (ADS) like the MYRRHA concept [13,14] and Generation IV advanced nuclear reactor concepts [15]. Reactor designs differ in fuel [16,17], neutron spectrum and thus fission product chemistry [18,19]. In Europe, mixed oxide fuel ($(U,Pu)O_2$) is the fuel of reference for LFRs [17]. Numerous fission products will form during operation, including the high-yield fission products Mo, together with Cs, Te and I. The mentioned fission products tend to migrate to the outer rim of the fuel pin [20], where they form a so-called JOG-layer above 7–8 % burn-up as found in post-irradiation experiments and thermochemical calculations for breeder reactors [20–22].

A thermodynamic model of the Pb-Mo-O is of interest for at least two reasons for the safety assessment of LFRs. First, in the accidental scenario of a clad breach, Mo-O containing fission product species may come into contact with Pb-coolant. Therefore, the Pb-Mo-O system is of interest in the modelling of the multi-element chemistry associated with clad breach in LFRs when oxide fuel, fission products and coolant will interact chemically [23]. Second, the system is important in the structural steel-coolant interactions, since Pb and the oxygen dissolved in it

* Corresponding author.
E-mail address: A.L.Smith@tudelft.nl (A.L. Smith).

https://doi.org/10.1016/j.jallcom.2024.175588
Received 19 April 2024; Received in revised form 4 July 2024; Accepted 15 July 2024
Available online 20 July 2024

can be corrosive for structural and cladding materials, which might be refractory Mo or Mo-containing steel. For the European Lead-cooled Fast Reactor (ELFR), the reactor vessel is made of austenitic stainless steel, while the fuel clad material is coated T91 [17]. Some types of austenitic steel contain up to 2.5 % Mo, while T91 contains approximately 1 % Mo. A study by Rivai *et al.* showed high corrosion resistance of Mo against LBE at 973 K [24,25]. However, after exposing refractory Mo to LBE at 873 K under oxygen-saturated conditions, Cairang and co-workers found formation of $PbMoO_4$ and Pb_2MoO_5 [26]. Thermodynamic studies into the Pb-Mo-O system have recently been performed to understand the formation and thermochemical stability of passive oxide films formed during operation [8,9], although some experimental gaps remain to be filled.

For these reasons, further experimental efforts and a thorough thermodynamic assessment are necessary. In this paper, both experimental and modelling work is reported. The low-temperature heat capacities of $PbMoO_4$ and Pb_2MoO_5 are measured using thermal relaxation calorimetry. Moreover, the melting enthalpy of $PbMoO_4$ is determined using differential scanning calorimetry. Third, thermal expansion studies on $PbMoO_4$ and Pb_2MoO_5 are reported based on high temperature X-ray diffraction measurements. The compounds are also studied using X-ray Absorption Near-Edge Structure spectroscopy at the Mo K-edge. The available thermodynamic data are assessed and CALPHAD (CALculation of PHAse Diagrams) modelling is performed, resulting in a full thermodynamic description of the Pb-Mo-O system.

2. Review of literature data on the Pb-Mo-O system

2.1. Constituting binary sub-systems

A thermodynamic description of the Pb-O system was published in 1999 by Risold *et al.* [27]. Since then, new experimental and modelling results were reported, which will be discussed below. A thermodynamic description of the Mo-O system is available in the TAF-ID database of the OECD/NEA [28]. For the Pb-Mo system, no thermodynamic description is known to the authors, though a tentative phase diagram was found [29]. The (x,T)-diagrams of the binary systems are shown in Fig. 1.

2.1.1. Binary Pb-O system

A thermodynamic modelling assesment of the Pb-O system was published in 1998 by Risold *et al.* [27]. This work assessed the thermodynamics of the Pb-O system, complementing a review of structural studies by Wriedt [30]. The Pb-O system includes the following binary compounds: PbO(L) (litharge, red), PbO(M) (massicot, yellow), Pb_3O_4, $Pb_{12}O_{17}$, $Pb_{12}O_{19}$ and PbO_2. Risold *et al.* modelled the liquid phase in the ionic two-sublattice model. Since the publication by Risold *et al.* in 1998, some additional thermodynamic investigations were reported.

Kobertz studied yellow PbO [31]. He reported vaporisation behaviour and measured the heat capacity of yellow PbO using DSC in the temperature range 298–1100 K. However, the heat capacity function for PbO he reported deviates significantly from previous results, see Figure S.1. Since the heat capacity value reached at melting cannot be matched to existing enthalpy increment data [32,33] and the total heat capacity as calculated using *ab initio* methods also supports the existing data set [34], the data set of Risold is retained. Moreover, Liu *et al.* did some DSC experiments in the Pb-PbO phase diagram [35]. Their results are in line with the phase diagram by Risold *et al.* [27].

Ganesan *et al.* measured the standard molar Gibbs free energy of formation of PbO(s) via electromotive force measurements (e.m.f.) [36]. The solubility of oxygen in liquid lead was investigated at least twice more: Ganesan *et al.* derived the solubility of oxygen in liquid Pb in the temperature range 815–1090 K from e.m.f. measurements [37], while Lim *et al.* studied the solubility of oxygen by coulometric titration [38] in the range 623–823 K. In 2005, a thermodynamic assessment of the ternary Cu-Pb-O system was published [39], in which the high-temperature equilibria between Pb and PbO were re-optimised compared to the assessment by Risold on the basis of a selection of available solubility data. This re-optimisation was deemed necessary to be able to model the ternary Cu-Pb-O system accurately. However, the solubility of oxygen in molten lead as recommended in the *Handbook on Lead-bismuth Eutectic Alloy and Lead Properties, Materials Compatibility, Thermohydraulics and Technologies* [40] is better reproduced by the model of Risold *et al.* In this work, the model of Risold *et al.* [27] and the selection of [40] are retained. A visualisation of the difference is given in Figure S.2.

It is important to note that we also found two typographic errors in the publication by Risold *et al.*. For $Pb_3O_4^{-T}$, the equation should read:

$$\begin{aligned} G(T) \quad = \quad & -802140 + 1112{\cdot}T/K - 194.5{\cdot}T/K{\cdot}\ln(T/K) \\ & -0.0025{\cdot}(T/K)^2 + 1566000{\cdot}(T/K)^{-1} \end{aligned} \tag{1}$$

where the fourth term changed sign. The function $G^{0,G}_{Pb}$ for $2000 < T < 3700$ K should have a minus sign for the term with T^2.

2.1.2. Binary Mo-O system

The thermodynamic description of the Mo-O system is taken from the work of Corcoran *et al.* [41], and the updated liquid phase parameters by Kauric [42]. In this model the compounds MoO_2, Mo_4O_{11}, Mo_8O_{23}, Mo_9O_{26} and MoO_3 are treated as stoichiometric. By using this model, we assure that the results of this study are consistent with work on the Ba-Mo-O system [43] as well as the international TAF-ID project [28].

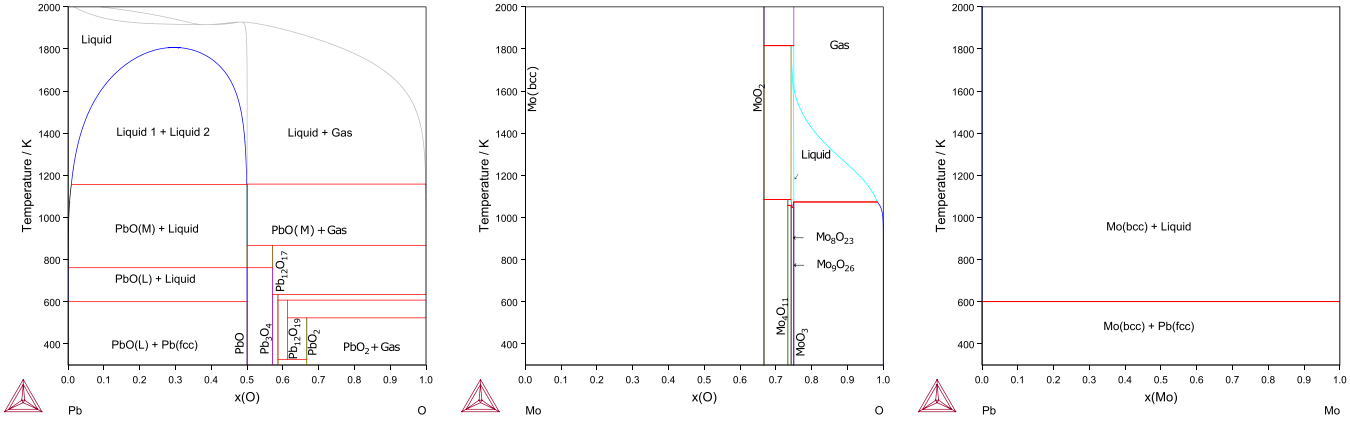

(a) Pb-O (b) Mo-O (c) Pb-Mo

Fig. 1. Binary phase diagrams used in the current work.

2.1.3. Binary Pb-Mo system

Mo is stable as bcc (A2) phase, while Pb is stable as fcc (A1) phase [44]. The metals are practically immiscible. A phase diagram of Mo-Pb is reported in the Landolt-Börnstein New Series [29]. As cited by [29], Parkman *et al.* found that less than 10^{-4} at% Mo is soluble in liquid Pb between 1150 and 1280 K, while Alden *et al.* found solubility of less than 0.011 at% Mo at 1479 K [45]. *Landolt-Börnstein* constructed its phase diagram based on estimations by Brewer *et al.* [46] and improvements by Massalski *et al.* [47]. Recently, two studies were published reporting co-deposition to form a film.[48,49] It seems possible to form a thin film or compound with composition Mo_3Pb, that is thermally stable up to a minimum of 523 K and a maximum of 573 K [48]. This phase is not taken into account in this assessment: first, it is not reported as bulk compound; second, no thermodynamic information is available; last, a LFR cooled with liquid Pb operates at temperatures above the melting point of lead, so this phase would not be thermally stable under operating conditions. The Pb-Mo system has been modelled herein using arbitrarily high thermodynamic parameters to destabilise the solution phases, as given in Table 1. The resulting phase diagram was already shown in Fig. 1.

2.2. Structural data for the ternary Pb-Mo-O phases

The number of compounds in the Pb-Mo-O system is rather limited. Recently, isotherms at 773 K and 998 K were investigated by Aiswarya *et al.* [8]. The reader is referred to their literature review for the discussion of the literature before 2017. Here, the structural data are summarised: $PbMoO_4$ and Pb_2MoO_5 are established for over a century [7], while Pb_5MoO_8 was for the first time reported in 1965 [50]. Later on, $PbMo_5O_8$ [51] and $Pb_3Mo_{16}O_{24}$ [52] were reported. Aiswarya *et al.* [8] tried to reproduce the syntheses reported for $PbMo_5O_8$ and $Pb_3Mo_{16}O_{24}$, but they were not able to synthesise $PbMo_5O_8$ using the reaction conditions reported by [51], nor using lower temperatures. $Pb_3Mo_{16}O_{24}$ was only partially found via synthesis at 1215 K for 240 h, starting from Mo, MoO_3 and $PbMoO_4$ in a closed ampoule. A similar result was found by Xu [53]. Aiswarya *et al.* also found that a synthesis temperature of 998 K is not enough [8]. According to Feja [54], the composition $Pb_3Mo_{16}O_{24}$ shifts to $PbMo_5O_8$ at 1523 K. Besides these compounds, the perovskite phase $PbMoO_3$ was also reported recently [55]. However, since $PbMoO_3$ is only reported to form as high temperature-high pressure phase, it is excluded from the present model. Moreover, experiments with partial reduction under hydrogen at 773 K and 998 K on $PbMoO_4$ resulted in a mixture of Pb, MoO_2 and $PbMoO_4$ [8].

Thus, the hexavalent phases $PbMoO_4$, Pb_2MoO_5 and Pb_5MoO_8 are left for consideration, together with the exotic couple $Pb_3Mo_{16}O_{24}$-$PbMo_5O_8$. The reported crystallographic data (at ambient pressure) for each phase are listed in Table 2. Pb_2MoO_5 and Pb_5MoO_8 are classified as compounds containing chains of OPb_4 tetrahedra [56]. The exotic couple $Pb_3Mo_{16}O_{24}$-$PbMo_5O_8$ was not included in the thermodynamic assessment, since Aiswarya *et al.* were not able to reproduce the claims of their formation [8] and because of the lack of experimental thermodynamic data. (In)homogeneity of the compounds was investigated for both $PbMoO_4$ [57] and Pb_2MoO_5 [58]. The small extent of the homogeneity range of $PbMoO_4$ (reported as 49.85–50.50 mol-% MoO_3) allows us to neglect this effect herein and treat the compounds as line compounds.

Table 1
Thermodynamic functions used in the model of the Pb-Mo system.

Phase	Gibbs energy ($J \cdot mol^{-1}$)	Ref.
fcc(A1)	$G[(Pb)(Va)] = G^{SER}_{Pb}$	[44]
	$G[(Mo)(Va)] = G^{fcc}_{Mo}$	[44]
	$L[(Mo, Pb)(Va)] = +300000$	This work
bcc(A2)	$G[(Pb)(Va)_3] = G^{bcc}_{Pb}$	[44]
	$G[(Mo)(Va)_3] = G^{SER}_{Mo}$	[44]
	$L[(Mo, Pb)(Va)_3] = +300000$	This work
Liquid	$L^0(Pb^{2+})_P(Va^{Q-})_Q = G^{Liq}_{Pb}$	[44]
	$L^0(Mo^{4+})_P(Va^{Q-})_Q = G^{Liq}_{Mo}$	[44]
	$L^0(Mo^{4+}, Pb^{2+})_P(Va^{Q-})_Q = +300000$	This work

Table 2
Crystallographic data at ambient pressure on the reported compounds in the Pb-Mo-O system.

Phase	Mo ox. state	Space group	Cell parameters (Å or°)	Ref.
$PbMoO_4$	+6	$I4_1/a$ (88)	$a = 5.424$ $c = 12.076$	[59]
Pb_2MoO_5	+6	$C2/m$ (12)	$a = 14.2221(11)$ $b = 5.7852(5)$ $c = 7.3262(6)$ $\beta = 114.168(2)$	[60]
Pb_5MoO_8	+6	$P2_1/c$ (14)	$a = 15.330(1)$ $b = 11.829(2)$ $c = 11.631(2)$ $\beta = 90.104(14)$	[61]
$PbMo_5O_8$	+2.8	$P2_1/c$ (14)	$a = 9.993(2)$ $b = 9.247(1)$ $c = 7.536(2)$ $\beta = 109.39(2)$	[51]
$Pb_3Mo_{16}O_{24}$	+2.625	$P4/mnc$ (128)	$a = 9.615(1)$ $c = 11.362(3)$	[52]

2.3. Thermodynamic data for ternary Pb-Mo-O phases

Of the *supra* selected compounds, thermodynamic data are only available for $PbMoO_4$ and Pb_2MoO_5, so these are the only two compounds discussed here. For reported melting temperatures, the reader is referred to Table 8.

2.3.1. $PbMoO_4$

The standard enthalpy of formation of $PbMoO_4$ was investigated many times, see Table 3; the most recent investigation is by Aiswarya *et al.* [9], who reviewed all earlier data. The data reported by Muldrow and Hepler [62], Dellien *et al.* [63], Bissengaliyeva *et al.* [64] and Aiswarya *et al.* [9], based on direct calorimetric measurements, are used to calculate a weighted mean that is selected as reference for the present thermodynamic model, yielding $\Delta_f H^\circ_m(PbMoO_4, cr, 298.15) = -(1052.9 \pm 0.5)\ kJ \cdot mol^{-1}$. The other values are not used in the current weighted mean, since they are already an assessment or because it was not a direct enthalpy measurement.

Table 3
Enthalpy of formation $\Delta_f H^\circ_m$ ($kJ \cdot mol^{-1}$) of $PbMoO_4$. The value for this work was calculated using Equations 1 and 2 in the Supporting Information. Uncertainties as reported by the original sources.[+] cited via [9]. * analysis in this work, see text for explanation.

Reference	$\Delta_f H^\circ_m$ (298.15 K)/ $kJ \cdot mol^{-1}$	Method
Muldrow & Hepler, [62]	-1049.1 ± 3.7	Heat of precipitation reaction calorimetry
Dellien *et al.*, [63]	-1052.66 ± 0.5	Solution calorimetry
Bissengaliyeva [64]	-1051.2 ± 4.3	High-temperature melt calorimetry
Aiswarya *et al.*, [9]	-1059.6 ± 2.2	Solution calorimetry
This work, assessment	$-$ **1052.9** $\pm$ **0.5**	Recommended, see text
Wagman *et al.*,[+]	-1051.9 ± 0.85	Compilation
O'Hare *et al.*,[+]	-1025.08	Estimation
Feja, [54]	-1042.1	Estimation
Aiswarya *et al.*, [8]	-1036.6 ± 0.7	e.m.f., 2nd law
Aiswarya *et al.*, [8]	-1055.5 ± 1.6	e.m.f., 3rd law *

The standard entropy of $PbMoO_4$ at 298.15 K is given in the NBS Tech Note 270–4 (1969) to be $S^\circ_m = 166.1\ J \cdot K^{-1} \cdot mol^{-1}$ [65], based on low temperature heat capacity measurements by Weller and Kelley (1964) in the temperature range 51–298 K [66]. Bissengaliyeva calculated a value of $S^\circ_m = (168.33 \pm 2.06)\ J \cdot K^{-1} \cdot mol^{-1}$ when measuring the low temperature heat capacity from 320 K down to 55 K [67]; when they also measured the region from 80 to 4.3 K, they obtained a value of $S^\circ_m = 161.5 \pm 0.3\ J \cdot K^{-1} \cdot mol^{-1}$ [64,68]. The latter value of Bissengaliyeva *et al.* is preferred over the former ones, since it includes actual measured data between 4.3 and 55 K. A calculation with all data, including new data obtained in this work, yielded for the standard entropy: $S^\circ_m = 160.9 \pm 0.3\ J \cdot K^{-1} \cdot mol^{-1}$, where the uncertainty has been estimated to be equal or better than the uncertainty reported by Bissengaliyeva *et al.* [68].

In 2017, Aiswarya *et al.* also published a study in which they carried out e.m.f. measurements, yielding the Gibbs energy of reaction between 772 and 1017 K [8]. As is given in Table 3, the enthalpy of formation at 298.15 K deduced using a second law analysis deviates from the other values. A third analysis performed in the current work yields a value closer to the selected value, but also a small drift was observed. The data is further discussed in the SI.

Heat capacity measurements at standard and high temperatures are reported by several authors. Weller and Kelley give a value of $C_p(298.15\ K) = (119.7 \pm 2.1)\ J \cdot K^{-1} \cdot mol^{-1}$ [66], while Bissengaliyeva *et al.* report $C_p(298.15\ K) = (119.4 \pm 0.13)\ J \cdot K^{-1} \cdot mol^{-1}$ [67]. Aiswarya *et al.* reported in 2018 heat capacity measurements using DSC over the temperature range 313–798 K [8]. At 298.15 K, the equation of Aiswarya *et al.* yields $C_p(298.15\ K) = 116.23\ J \cdot K^{-1} \cdot mol^{-1}$.

To avoid a small mismatch between low- and high-temperature heat capacity data, the heat capacity function was fitted anew to both the high-temperature data and a part of the low-temperature data:

$$C_p/J{\cdot}K^{-1}{\cdot}mol^{-1} = 112.192 + 65.55{\cdot}10^{-3}{\cdot}T/K - 965693{\cdot}(T/K)^{-2} - 2.317{\cdot}10^{-5}{\cdot}(T/K)^2 \quad (2)$$

with $C_p(298.15\ K) = 118.8\ J \cdot K^{-1} \cdot mol^{-1}$.

2.3.2. Pb_2MoO_5

The enthalpy of formation is estimated by Feja to be $\Delta_f H^\circ_m(Pb_2MoO_5, cr, 298.15) = -1294.6\ kJ \cdot mol^{-1}$ [54]. More recently, Aiswarya *et al.* reported the enthalpy of formation as determined by solution calorimetry to be $\Delta_f H^\circ_m(Pb_2MoO_5, cr, 298.15) = -(1274.7 \pm 2.3)\ kJ \cdot mol^{-1}$ [9]. These two values are the only values known. The value of Aiswarya *et al.* is favoured, since it is based on experimental measurement.

The standard entropy at 298.15 K was estimated by Feja to be $S^\circ_m = 209\ J \cdot K^{-1} \cdot mol^{-1}$ [54]. This is in the expected order of magnitude as calculated from the method of Glasser [69], yielding $215.4\ J \cdot K^{-1} \cdot mol^{-1}$. No experimental data (low temperature heat capacity) are reported until now; *infra* the value obtained in the current work will be discussed, *viz.* $S^\circ_m = (244.8 \pm 7.4)\ J \cdot K^{-1} \cdot mol^{-1}$.

In 2017, Aiswarya *et al.* published a study where they performed e.m.f. measurements, yielding the Gibbs energy of reaction between 741 and 1021 K [8]. Again, these e.m.f. results are discussed in-depth in the SI.

The heat capacity at high temperature was reported twice. In 2004, Feja published an estimation [54]. Aiswarya published in 2018 a measurement using DSC in the range 308–798 K [9].

$$C_p \pm 6.2/J{\cdot}K^{-1}{\cdot}mol^{-1} = 169.20 + 66.69{\cdot}10^{-3}{\cdot}T/K - 1.99{\cdot}10^{6}{\cdot}(T/K)^{-2} \quad (3)$$

At 298.15 K, the equation of Aiswarya *et al.* yields $C_p(298.15\ K) = 166.7\ J \cdot K^{-1} \cdot mol^{-1}$. This curve matches well with the low temperature heat capacity measured in this work (*vide infra*), so this fit is retained.

2.3.3. Thermodynamic properties of gaseous species

A mass spectrometry study was reported by Nikolaev *et al.* [70]. The authors refer to three earlier publications that report that upon heating $PbMoO_4$(s), mass spectrometric investigations indicate that congruent vaporisation, *i.e.* $PbMoO_4(s) = PbMoO_4(g)$ is practically the only occurring process. They conclude the gas phase over lead molybdate to consist mostly of $PbMoO_4$(g) molecules, but also of minor amounts of $PbMo_2O_7$(g), Pb_2MoO_5(g), Mo_3O_9(g), Pb_2O_2(g), PbO(g) and atomic Pb (g).

A combined mass spectrometry and density functional study of the gas phase of the PbO-MoO_3 system was published by Kunkel *et al.* [71] more recently. The authors made three samples, mixing PbO and MoO_3 in the ratios (2:3), (1:1) and (3:1). They detected four parent ions ($PbMo_3O^+_{10}$, $PbMo_2O^+_7$, $PbMoO^+_4$ and $Pb_2Mo_2O^+_7$). They also compare the experimental enthalpies of formation of the gaseous molecules with quantum chemical calculations. Important thermodynamic results are reproduced in Table S.1. To the best of our knowledge, no function of experimental vapour pressure against temperature is reported in the literature.

2.4. Phase diagram data in the Pb-Mo-O system

Over the time span of a century, several phase diagram studies were reported. Combined, they provide a rather well-established insight into the pseudo-binary section PbO-MoO_3, while leaving some open questions for some specific regions. The first report is by Jaeger and Germs (1921), who investigated the phase diagram section PbO-$PbMoO_4$ [7]. Besides the end-members, they found Pb_2MoO_5. Belyaev and Smolyaninov (1962) report the whole section PbO-MoO_3 [72]. The authors found the same compounds as Jaeger and Germs. Kunev *et al.* published a paper in 1966 on the MoO_3-$PbMoO_4$ system [73]; they found a single eutectic. The existence of Pb_5MoO_8 was first reported in 1965 by Doyle and Forbes [50]. Bukhalova *et al.* studied the section PbO-MoO_3 in 1971 [74] and reported only $PbMoO_4$ and Pb_2MoO_5. Eissa *et al.* reported in 1996 on the phase diagram PbO_2-Pb-MoO_3 in air [75]. Nihtianova *et al.* studied the Pb_5MoO_8 crystal growth together with the phase diagram closely to the Pb_5MoO_8 composition in 1997 [76].

Feja (2004) investigated the phase fields in the Pb-Mo-O section [54]. The author investigated the oxygen rich phase field, which is above the line Pb-MoO_2. Given the temperatures necessary to synthesise ternary compounds, the lead oxides of concern are limited to PbO and Pb_3O_4. Phase fields Pb_3O_4-MoO_3-$PbMoO_4$ and Pb_3O_4-$PbMoO_4$-Pb_2MoO_5 were found to be unstable at 773 K and atmospheric pressure. At 773 K, the coexistence line Pb_2MoO_5-Pb_3O_4 was found to exist, besides the section PbO-MoO_3. Within the Pb-MoO_2-MoO_3-PbO boundaries and at 774 K, lines between Pb and Pb_5MoO_8, Pb and Pb_2MoO_5, and Pb and $PbMoO_4$ were found, besides the $PbMoO_4$-MoO_2 line. Aiswarya *et al.* studied the phase fields of the Pb-Mo-O section at 773 and 998 K in 2017 [8]. They focused on the field between Pb-PbO-MoO_3-Mo. At 773 K, they found the compound Pb_5MoO_8 to be not (yet) stable. At 998 K, it was found to be stable.

2.5. Thermodynamic modelling assessment

Feja applied a modelling approach in his study of the Pb-Mo-O system [54] using Redlich-Kister-Murkschano-models for the liquid phase, but no parameters were reported. The Mo(VI)-compounds $PbMoO_4$, Pb_2MoO_5 and Pb_5MoO_8 are included, as well as an attempt to model the $PbMo_5O_8$ phase.

2.6. Thermal expansion studies

Some crystallographic studies into $PbMoO_4$ and Pb_2MoO_5 at non-ambient temperature are reported in the literature. For $PbMoO_4$, the crystal structure was studied using X-ray diffraction in the range 303–623 K [77]. The average coefficients of linear thermal expansion were found to be $\alpha_a = 12.19 \cdot 10^{-6}\ K^{-1}$ and $\alpha_c = 24.45 \cdot 10^{-6}\ K^{-1}$. The

authors cite unpublished work that reported $\alpha_a = 10.38 \cdot 10^{-6}\ K^{-1}$ and $\alpha_c = 25.31 \cdot 10^{-6}\ K^{-1}$ using interferometric measurements. The anisotropy of thermal expansion found was stated to be common in other compounds with the scheelite structure. Recently, Achary *et al.* used neutron diffraction to study the evolution of the lattice parameters between 5 and 300 K [78]. They found the average axial thermal expansion coefficients in this temperature region to be $\alpha_a = 9.39 \cdot 10^{-6}\ K^{-1}$ and $\alpha_c = 20.61 \cdot 10^{-6}\ K^{-1}$. The volumetric thermal expansion is plotted for comparison in Fig. 5. For completeness, the first study reporting linear thermal expansion is mentioned here too: Argyle *et al.* measured the dilation of $PbMoO_4$ [79], but it is unclear how to use and how to compare their reported data as to the other data, since $PbMoO_4$ expands anisotropiccally. If their data is taken as unity for α_a and multiplied by an anisotropy factor of 2.5 for α_c, their data agrees with the data obtained in the current work; this reading of their paper remains speculative, however. Therefore, we did not include their data in Fig. 5.

The crystal structure of $PbO.PbXO_4$ with X = S, Cr, Mo at 5 K was reported by Mentzen et al. [80], using neutron diffraction. To the best of our knowledge, this is the only diffraction study of Pb_2MoO_5 at non-ambient temperature.

3. Experimental

3.1. Synthesis

The chemicals $PbMoO_4$ (Merck Sigma, 99.9 %), PbO (Merck Sigma, 99.999 %) and MoO_3 (Alfa Aesar, 99.95 %) were purchased. Pb_2MoO_5 was synthesised via solid state synthesis by mixing PbO and MoO_3 in a 2:1 ratio. The mixture was ground and heated to 873 K under oxygen atmosphere in an alumina boat, where it was kept for 12 h. The sample was subsequently cooled to room temperature and reground, after which the heat treatment was repeated.

3.2. X-ray diffraction

Formation and purity of the compounds was confirmed by X-ray powder diffraction (XRD), using a PANalytical X'Pert PRO X-ray diffractometer mounted in the Bragg-Brentano configuration with a Cu-anode. The data were collected using an X'celerator detector. The samples were loaded in airtight sample holders closed with Kapton foil to prevent lead powder spreading. An XRK-900 furnace was used to heat the sample from ambient temperature up to 1173 K for $PbMoO_4$ and 1073 K for Pb_2MoO_5. Structural analysis was performed on the diffraction patterns using the profile refinement method [81,82] in the FullProf suite [83].

3.3. X-ray absorption near edge structure spectroscopy

X-ray Absorption Near Edge Structure (XANES) spectroscopy measurements were performed for MoO_2, MoO_3, $PbMoO_4$ and Pb_2MoO_5 at the INE beamline [84] of the KIT Light Source (Karlsruhe, Germany) with 2.5 GeV and 150–170 mA as operating conditions in the KARA storage ring. The beamline uses a Ge(422) double-crystal monochromator (DCM). Rh-coated mirrors located before (flat, cylindrically bent) and after (toroidal) the DCM are used to collimate and focus the synchrotron beam, respectively, producing a spot size of 500 μm by 500 μm at the sample surface. Transmission and fluorescence geometries could be measured in unison. Samples were probed around the K-edge of Mo (20 keV). The samples were prepared by mixing the compound with boron nitride (BN), which around the Mo K-edge is almost transparent to X-rays. The samples mixed with BN were pressed into a circular pellet of 8 mm diameter and enclosed in Kapton foil.

The energy E_0 of the edge absorption threshold position was taken at the inflection point of the spectrum using the the zero-crossing of the second derivative. The position of the pre-peak was selected as the peak maximum, using the first derivative. Several acquisitions were performed on the same sample and summed up to improve the signal-to-noise ratio. Before averaging the scans, each spectrum was aligned using the XANES spectrum of a metallic molybdenum reference foil measured simultaneously with the sample. The ATHENA software [85] was used to normalise and analyse the spectra.

3.4. Differential scanning calorimetry

Differential scanning calorimetry (DSC) measurements were performed using a Setaram Multi-Detector HTC Module of the 96 Line calorimeter with 3D heat flux detection. The temperature was calibrated by measuring the melting points of standard high purity metals (In, Sn, Pb, Al, Ag, Au). Open alumina crucibles were used under oxygen flow at ambient pressure with a heating rate of 10 K/min. The melting point of the compound was based on the determination of the onset temperature of the event. The estimated uncertainty per measurement is ± 5 K. The enthalpy of melting was determined by placing Cs_2MoO_4 as reference material with a polymorphic and a melting transition with known transition enthalpies [86] in the reference crucible, and measuring both sample and reference materials in the same cycle. The detector sensitivity s_{ref} for each measurement is equal to:

$$s_{ref} = \frac{M_{ref} \cdot A_{ref}}{m_{ref} \cdot \Delta_{tr} H_m^{\circ}(T_{tr,ref})} \quad (4)$$

where s_{ref} is in $\mu V \cdot mW^{-1}$, M_{ref} the molar mass of the reference material in $g \cdot mol^{-1}$, A_{ref} the area of the reference sample signal in $\mu V \cdot s$, m_{ref} the sample mass in mg, and $\Delta_{tr} H_m^{\circ}(T_{tr,ref})$ the transition or melting enthalpy of the reference in $J \cdot mol^{-1}$.

3.5. Low-temperature heat capacity and magnetic susceptibility

The low-temperature heat capacity was measured on two instruments, namely a Physical Property Measurement System from Quantum Design (QD-PPMS 14 T) and a Versalab equipment system from Quantum Design. The results were collected with zero field in the temperature range 2–300 K with slight variation of the precise temperature window per sample. The samples were thermally connected to the puck platform using Apiezon N-grease. First, a so-called addenda-curve was measured, giving the heat capacity of the sample puck and the thermal grease. After loading the sample on the puck, the total heat capacity was determined from which the sample heat capacity was extracted. All measurements were performed at very high vacuum (10^{-9} bar). The heat capacity of the sample was obtained by subtracting the addenda-curve from the total heat capacity, a procedure that is done by the software of the instruments (Multiview from Quantum Design). The heat capacity of $PbMoO_4$ was measured on a 3.05(5) mg sample using QD-PPMS systems of QuantumDesign. Pb_2MoO_5 samples have been measured on the QD-PPMS (full range) and Versalab (50–300 K) on pellets weighing 11.21(5), 12.79(5) and 13.40(5) mg respectively. The 12.79(5) mg sample has been encapsulated in Stycast 2850 FT to a total mass of 13.50(5) mg to improve thermal coupling and reduce potential interaction with atmosphere during installation on the sapphire platform of the QD-PPMS [87]. Heat capacity of Stycast 2850 FT is measured separately and subtracted to obtain the heat capacity of the sample. A 3 % uncertainty on the heat capacity has been used in the error analysis as a conservative error estimate [88,89].

The non-encapsulated samples were afterwards measured in a Quantum Design MPMS-7 device to study the magnetic susceptibility. Measurements have been performed by fixing pellets on a low magnetic contribution quartz support and measured in DC magnetic field up to 70 kOe applied field and varying temperature from 2 to 300 K. Both materials present diamagnetic features and almost temperature independent behaviour.

4. Thermodynamic models

To optimise the thermodynamic parameters of the Pb-Mo-O model with the CALPHAD approach, the PARROT module of the ThermoCalc software (Version 2023b) was used [90,91]. The three hexavalent lead molybdates were treated as stoichiometric compounds. The Gibbs energy functions of all the phases are referred to the enthalpy of the pure elements in their stable state at standard conditions, *i.e.* 298.15 K and 1 bar and the temperature-dependent terms are in Kelvin.

4.1. Pure elements

The Gibbs energy functions of the pure elements Pb, Mo and O at temperature T and in state ϕ with parameters as reported by Dinsdale [44] follow the general equation:

$$G_i^{\phi}(T) - {}^{\circ}H_i^{SER}(298.15K) = a + b{\cdot}T + c{\cdot}T{\cdot}\ln T + \sum d_n T^n \quad (5)$$

where $n \in \{2, 3, -1, \ldots\}$. Metallic Pb was included in the description of the fcc (A1) phase with sub-lattices (Pb,Mo)(O,Va) (Va being a vacancy), while molybdenum is stable as bcc (A2) phase with sub-lattices (Mo,Pb, Va)(O,Va)$_3$.

4.2. Binary oxides

The binary oxides of the Mo-O system (MoO_2, Mo_4O_{11}, Mo_8O_{23}, Mo_9O_{26}, MoO_3) and of the Pb-O (PbO, Pb_3O_4, $Pb_{12}O_{17}$, $Pb_{12}O_{19}$ and PbO_2) system were described as stoichiometric compounds; the Gibbs energy functions have the same form as Equation (5):

$$G^{\phi}(T) - \sum_i n_i^{\phi} {}^{\circ}H_i^{SER}(298.15K) = a + b{\cdot}T + c{\cdot}T{\cdot}\ln T + \sum d_n T^n \quad (6)$$

where n_i^{ϕ} is the number of atoms of the element in the formula. The functions were taken from Corcoran *et al.* and Kauric [41–43] and Risold *et al.* [27] for Mo-O and Pb-O oxides, respectively.

4.3. Hexavalent ternary molybdates

The complex molybdates formed on the section PbO-MoO_3 were described with a three-sub-lattice model of the form $(Pb^{2+})_x(Mo^{6+})_y(O^{2-})_{x+3y}$. The mathematical form of the Gibbs energy is equivalent to Equation (6). As a starting point, available experimental enthalpy of formation, entropy and heat capacity data were used to express the Gibbs energy functions for $PbMoO_4$ and Pb_2MoO_5. Pb_5MoO_8, for which no experimental thermodynamic data is available, was modelled using a combination of the Gibbs energy functions of Pb_2MoO_5 and PbO matching its stoichiometry, after which its enthalpy and entropy at 298.15 K were optimised.

4.4. Liquid phase

The ionic two sub-lattice model as proposed by Hillert et al. [92] was used to describe the liquid phase. The first lattice in this model contained the cationic species, while the second lattice contained anionic and neutral species, including vacancies:

$$(Mo^{4+}, Pb^{2+})_P(MoO_4^{2-}, O^{2-}, Va^{Q-}, MoO_3, O)_Q \quad (7)$$

with P and Q equal to the average charge of the opposite sub-lattice:

$$P = 2y_{MoO_4^{2-}} + 2y_{O^{2-}} + Qy_{V\,a^{Q-}} \quad (8)$$

$$Q = 2y_{Pb^{2+}} + 4y_{Mo^{4+}} \quad (9)$$

where the various site fractions are described with the respective y's.

The Gibbs energy of the liquid phase for any composition in the Pb-Mo-O system is given by the sum of the reference terms of the end-member species (Pb, Mo, O, $PbMoO_4$, …) multiplied by their fractions, a configurational entropy term on the cationic and the anionic lattices and an excess term:

$$\begin{aligned} G^{\text{liquid}} = {} & y_{Pb^{2+}}y_{MoO_4^{2-}}\,{}^{\circ}G_{(Pb^{2+})_2(MoO_4^{2-})_2} + y_{Pb^{2+}}y_{O^{2-}}\,{}^{\circ}G_{(Pb^{2+})_2(O^{2-})_2} \\ & + Qy_{Pb^{2+}}y_{V\,a^{Q-}}\,{}^{\circ}G_{(Pb^{2+})_1(V\,a^{1-})_2} + y_{Mo^{4+}}y_{MoO_4^{2-}}\,{}^{\circ}G_{(Mo^{4+})_2(MoO_4^{2-})_4} \\ & + y_{Mo^{4+}}y_{O^{2-}}\,{}^{\circ}G_{(Mo^{4+})_2(O^{2-})_4} + Qy_{Mo^{4+}}y_{V\,a^{Q-}}\,{}^{\circ}G_{(Mo^{4+})_1(V\,a^{1-})_4} \\ & + Qy_{MoO_3}\,{}^{\circ}G_{MoO_3} + Qy_O\,{}^{\circ}G_O \\ & + RT\Big(P\big[y_{Pb^{2+}}\ln(y_{Pb^{2+}}) + y_{Mo^{4+}}\ln(y_{Mo^{4+}})\big] \\ & + Q\Big[y_{MoO_4^{2-}}\ln\left(y_{MoO_4^{2-}}\right) + y_{O^{2-}}\ln(y_{O^{2-}}) \\ & + y_{V\,a^{Q-}}\ln(y_{V\,a^{Q-}}) + y_{MoO_3}\ln(y_{MoO_3}) + y_O\ln(y_O)\Big]\Big) + G^{\text{excess}} \end{aligned} \quad (10)$$

The excess Gibbs energy parameters used in this model are $L^0(Pb^{2+})_P(MoO_4^{2-}, O^{2-})_Q$ and $L^1(Pb^{2+})_P(MoO_4^{2-}, O^{2-})_Q$ for the PbO-$PbMoO_4$ range, and $L^0(Pb^{2+})_P(MoO_4^{2-}, MoO_3)_Q$ and $L^1(Pb^{2+})_P(MoO_4^{2-}, MoO_3)_Q$ for the $PbMoO_4$-MoO_3 range.

4.5. Gas phase

The gas phase is described by an ideal mixture of Mo, Mo_2, Mo_2O_6, Mo_3O_9, Mo_4O_{12}, Mo_5O_{15}, MoO, MoO_2, MoO_3, O, O_2, O_3, Pb, Pb_2, Pb_2O_2, Pb_3O_3, Pb_4O_4, Pb_5O_5, Pb_6O_6, PbO, $PbMoO_4$, Pb_2MoO_5, $PbMo_2O_7$ and $PbMo_3O_{10}$. The corresponding Gibbs energy G^{ϕ} reads:

$$G^{\phi} = \sum_i y_i^{\circ}G_i^{\phi} + RT\sum_i y_i \ln y_i + RT\ln\frac{P}{P^0} \quad (11)$$

where the first term includes the fraction of the gas species at any point in the system multiplied by the Gibbs energy of the gaseous species i, the second term is a mixing entropy term, and the third term the pressure influence as normalised on standard pressure P^0. The Gibbs energy expression of the species $PbMoO_4$(g), $PbMo_2O_7$(g), Pb_2MoO_5(g), and $PbMo_3O_{10}$(g) are taken from Kunkel *et al.* [71].

5. Results and discussion

5.1. Structural analysis

The obtained diffraction patterns for $PbMoO_4$ and Pb_2MoO_5 are shown in Figs. 2 and 3, respectively. No unaccounted peaks were found

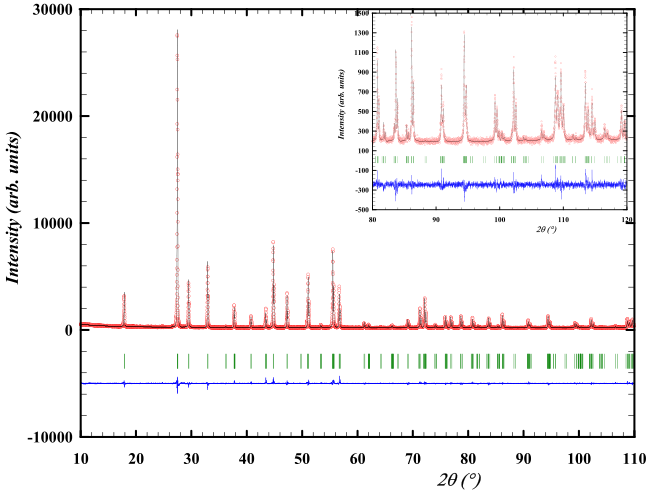

Fig. 2. Experimental (Y_{obs}, in red) and calculated (Y_{calc}, in black) XRD patterns of $PbMoO_4$ at ambient temperature. The difference between calculated and experimental intensities $Y_{obs} - Y_{calc}$ is shown in blue. The angular positions of Bragg reflections are shown in green. Measurement at λ = Cu K_{α}.

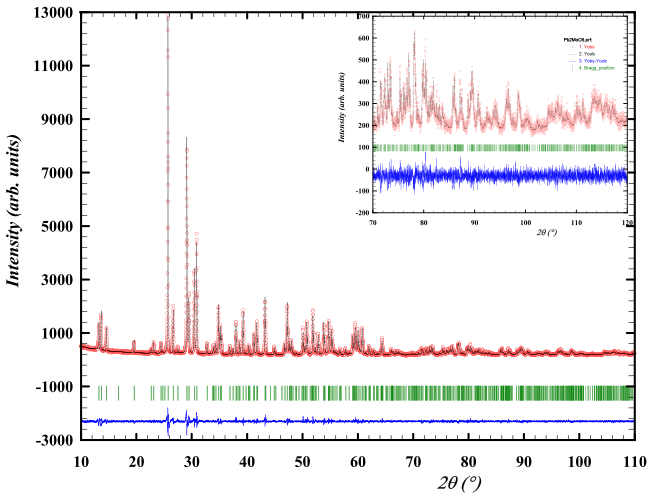

Fig. 3. Experimental (Y_{obs}, in red) and calculated (Y_{calc}, in black) XRD patterns of Pb_2MoO_5 at ambient temperature. The difference between calculated and experimental intensities $Y_{obs} - Y_{calc}$ is shown in blue. The angular positions of Bragg reflections are shown in green. Measurement at λ = Cu K_α.

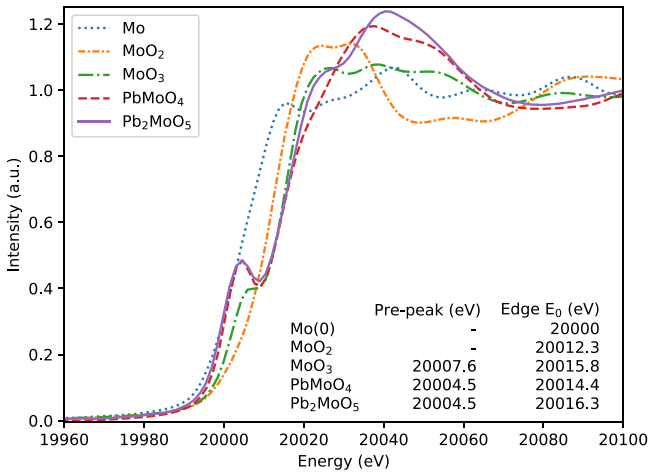

Fig. 4. X-ray Absorption Near-Edge Structure (XANES) spectra around the Mo K-edge with energy values of the pre-peak and edge in the normalised XANES spectra. The edges are determined based on the inflection points in the normalised XANES spectra at the Mo K-edge. The pre-peaks are determined via the maximum.

on the X-ray diffraction patterns. The refined cell parameters as obtained in the space groups $I4_1/a$ (88) and $C2/m$ (12) respectively, are listed in Table 4. The cell parameter values are in line with those reported in literature, *e.g.* the values in Table 2.

5.2. X-ray absorption spectroscopy

Oxidation states of the molybdates were studied using X-ray Absorption Near Edge Structure (XANES) spectroscopy. Since, to the best of our knowledge, no XANES measurements on Pb_2MoO_5 were reported previously, the Pb_2MoO_5 K-edge was probed and is shown in Fig. 4. In this figure, Pb_2MoO_5 is compared to Mo^0, $Mo^{IV}O_2$, $Mo^{V\ I}O_3$ and $PbMo^{V\ I}O_4$. The derived absorption edge threshold and pre-peak features are listed in the table in Fig. 4. The measured E_0 value for Pb_2MoO_5 is close to that of $PbMoO_4$ and MoO_3, indicating a valence state +6. The intrinsic features of Mo^0, Mo^{IV}, $Mo^{V\ I}$ can be seen in the increase in E_0-position with increasing Mo valence state. Moreover, while Mo and MoO_2 have a simple edge, Mo(VI) in MoO_3 has a characteristic pre-edge feature. This pre-edge feature is also found in $PbMoO_4$ and Pb_2MoO_5. The pre-edge feature originates from the tetrahedral environment of the oxygen atoms around the Mo centre [93,94].

5.3. Thermal expansion

The volumetric thermal expansion of $PbMoO_4$ is plotted in Fig. 5. As can be seen in this figure, the current data between 298 K and 1173 K is in line with the data reported by Suryanarayana and Deshpande [77] and joins with the low-temperature data of Achary et al. [78]. In the inset of Fig. 5, the expansion of the cell parameters a (=b) and c relative to 298 K is shown. Based on this fit, the thermal expansion values between 298 and 1173 K of the a- and c-axes are given by $12.3 \cdot 10^{-6}$ K^{-1} and $30.5 \cdot 10^{-6}$ K^{-1}. Using the same fitting method, the volumetric thermal expansion gives $56 \cdot 10^{-6}$ K^{-1}. As can be seen from the fits, the behaviour is slightly non-linear: upon increasing temperature, the

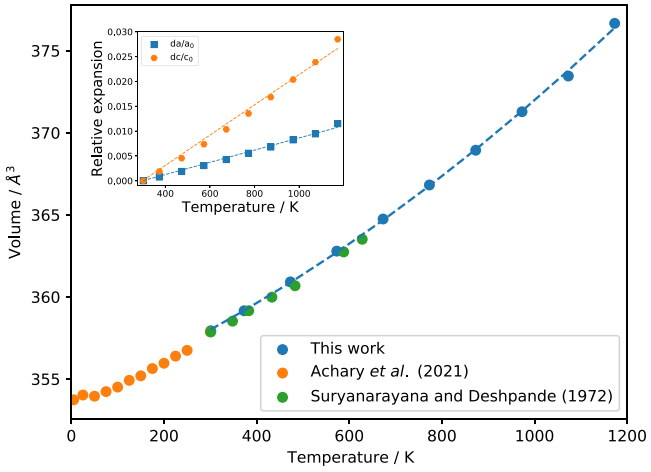

Fig. 5. Volumetric thermal expansion of $PbMoO_4$ as measured in this work (blue), by Achary *et al.* [78] and by Suryanarayana and Deshphande [77]. The inset shows the relative lattice parameter expansion on the a- and c-axes.

increase in cell parameter and thus volume increases. The volume of $PbMoO_4$ is best described with the second order polynomial:

$$V(T)/\mathrm{nm}^3 = 353.9 + 0.0117 \cdot T/K + 6.34 \cdot 10^{-6} \cdot (T/K)^2 \quad (12)$$

with temperature in Kelvin. Overall, the parameters obtained in this work are consistent with the values found in literature as discussed *supra*. The lattice parameters at non-ambient temperature are given in Table S.2.

The volumetric thermal expansion of Pb_2MoO_5 is plotted in Fig. 6. Pb_2MoO_5 crystallises in the monoclinic space group $C2/m$ (12). The a-axis evolves linearly with temperature, while the expansion of the b and c axis are non-linear. Describing the whole temperature range 298 K till 1073 K linearly, one obtains for the thermal expansion coefficient of the lattice parameters a, b and c, $8.6 \cdot 10^{-6}$ K^{-1}, $29 \cdot 10^{-6}$ K^{-1} and $40 \cdot 10^{-6}$ K^{-1}, respectively. Using a polynomial of degree 2, the volume of Pb_2MoO_5 is described by:

$$V(T)/\mathrm{nm}^3 = 540 + 0.0295 \cdot T/K + 1.21 \cdot 10^{-5} \cdot (T/K)^2 \quad (13)$$

The cell parameters at non-ambient temperature are given in

Table 4
Refined cell parameters of the powders used in this research as found from the X-ray diffraction data for respectively $PbMoO_4$ and Pb_2MoO_5. Both compounds have $Z = 4$. .

Compound	a (Å)	b (Å)	c (Å)	β(°)
$PbMoO_4$	5.4365(10)	5.4365(10)	12.1109(3)	90
Pb_2MoO_5	14.2168(5)	5.7866(2)	7.3292(2)	114.142(2)

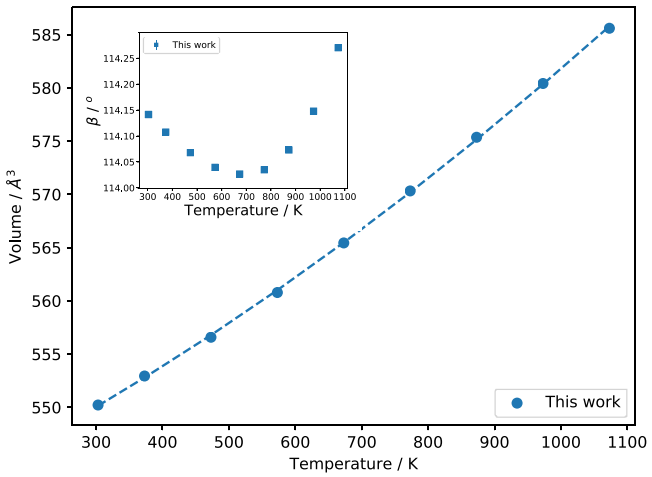

Fig. 6. Volumetric thermal expansion of Pb_2MoO_5 as measured in this work (blue). The inset shows the evolution of angle β with increasing temperature.

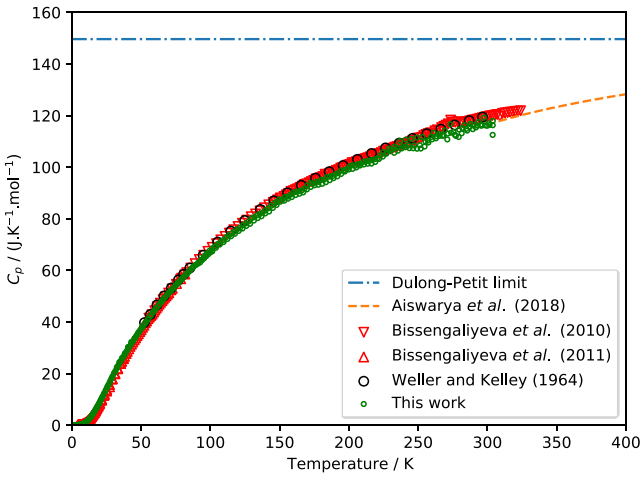

Fig. 7. Low temperature heat capacity of $PbMoO_4$ as measured by Weller and Kelley [66], Bissengaliyeva *et al.* [67,68] and in this work, as compared to the high-temperature heat capacity as measured by Aiswarya *et al.* [9] and the Dulong-Petit limit.

Table S.3.

5.4. Melting enthalpy $PbMoO_4$

The enthalpy of melting of $PbMoO_4$ was measured 4 times against the enthalpy of transition and enthalpy of melting of Cs_2MoO_4 [86]. The results are shown in Table 5. The enthalpy of the solid-liquid transition was calculated using the sensitivity factor as given in Equation (4). The obtained melting enthalpy is (62.3 ± 3) kJ · mol^{-1} with the corresponding melting point (1338 ± 5) K. A similar analysis using the α-Cs_2MoO_4 = β-Cs_2MoO_4 transition yields (66.7 ± 3) kJ · mol^{-1}. The former value is preferred since the melting temperature of Cs_2MoO_4 is closer to the melting temperature of $PbMoO_4$, so the derived sensitivity is expected to be more accurate.

5.5. Low-temperature heat capacity and magnetic susceptibility of $PbMoO_4$ and Pb_2MoO_5

The low-temperature heat capacity of $PbMoO_4$ is shown in Fig. 7. The results obtained in this work agree well with literature. The small anomaly as reported by Bissengaliyeva *et al.* [68] at 273 K was not observed in this work and might be attributed to water, because there seems to be no structural or other physical reason to have any transition inherent to $PbMoO_4$. This means the *supra* selected entropy value can be retained. In Figure S.3, the magnetic susceptibility is shown, confirming the absence of any anomaly in the studied temperature range. In this work, the heat capacity between 2 and 4 K has been measured for the first time. Figure S.5 confirms that only lattice contributions to the heat capacity are present.

The low-temperature heat capacity of Pb_2MoO_5 is shown in Fig. 9. The low-temperature data match with the high-temperature data as reported by Aiswarya *et al.* [8]. The heat capacity at 298.15 K obtained here equals C_p(298.15 K) = (172 ± 5) J · K^{-1} · mol^{-1}, which is in line with the extrapolation from the high-temperature heat capacity of Aiswarya *et al.* [9], *viz.* (166.7 ± 6.2) J · K^{-1} · mol^{-1}. The lower temperature range was plotted, as shown in Figure S.5. As can be concluded from this fit, there is no electronic contribution to the heat capacity, as expected for an insulating material. In Figure S.4, the magnetic susceptibility is shown, confirming the absence of any anomaly in the studied temperature range. The data of the 11.21(5) mg sample joins best with the data of Aiswarya *et al.* at higher temperatures. The sample of 12.79(5) mg was encapsulated in stycast, which adds an extra error source. Typically, the corresponding uncertainty on the heat capacity can be estimated to be 3 %. To obtain the standard entropy at 298.15 K, the curve of the 11.21(5) mg sample was selected; extension below 50 K was done using the curve of the 12.79(5) mg sample joint to the 11.21(5) mg sample curve. A standard entropy at 298.15 K of (244.8 ± 7.4) J · K^{-1} · mol^{-1} was obtained. Integration of the curve obtained on the 12.79(5) mg sample on itself yields (252 ± 7) J · K^{-1} · mol^{-1}, which is just within error limits of the selected curve. The third curve is in line with the other two samples, but is only measured between 50 and 200 K and therefore not used for entropy determination at 298.15 K. Thus, the entropy used in this work is S°_m(298.15 K) = (244.8 ± 7.4) J · K^{-1} · mol^{-1}.

Table 5
Experimental results of the DSC measurements of $PbMoO_4$(s)=$PbMoO_4$(l) versus β − Cs_2MoO_4(s)=Cs_2MoO_4(l). The average and standard deviation are calculated using Equations 1 and 2 in the Supporting Information.

m_{PbMoO_4} (mg)	T_{tr} (K)	$m_{Cs_2MoO_4}$ (mg)	A_{sample} (μV · s)	A_{ref} (μV · s)	s_{ref} (μV · mW^{-1})	$\Delta_{tr}H^\circ_m$ (kJ · mol^{-1})
74.10	1338.4	39.89	70.24	16.25	0.00545	63.8 ± 5
76.05	1338.7	67.59	70.01	28.27	0.00560	60.4 ± 6
50.89	1336.9	63.88	71.52	39.89	0.00836	61.7 ± 8
49.43	1338.3	67.66	75.34	44.74	0.00885	63.2 ± 8
Average	1338 ± 5					62.3 ± 3

6. Thermodynamic modelling assessment

6.1. Optimised parameters

The optimised parameters for the Pb-Mo-O system are summarised in Table 6.

6.2. Thermodynamic data

The selected and optimised enthalpies of formation and standard entropy are compared in Table 7. The selected values for $PbMoO_4$ and Pb_2MoO_5 allow for a successful optimisation, proving the consistency of the data. No experimental data for Pb_5MoO_8 was available, so no comparison can be made.

The melting enthalpy of $PbMoO_4$ as found in the optimised model equals 59.9 kJ · mol^{-1} at 1346 K (measured: (62.3 ± 3 kJ · mol^{-1}) at 1338 ± 5 K). The calculated melting enthalpy of Pb_2MoO_5 equals 80.6 kJ · mol^{-1} at 1215 K.

The heat capacities of $PbMoO_4$ and Pb_2MoO_5 as used in the model are plotted in Figs. 8, 9 and 10.

Table 6
Thermodynamic functions used in the optimisation of the Pb-Mo-O model. Optimised values are given in **bold**.

Phase	Gibbs energy (J · mol^{-1})	Ref.
Liquid	${}^{\circ}G(Pb^{2+})_2(MoO_4^{2-})_2 - 2{}^{\circ}H^{SER}_{Pb} - 2{}^{\circ}H^{SER}_{Mo}$	This work
	$-8{}^{\circ}H^{SER}_{O} = 2G_{PbMoO_4} + \mathbf{41600–26.6} \cdot T$	
	$L^0(Pb^{2+})_P(MoO_4^{2-},O^{2-})_Q = \mathbf{+171000–196.7} \cdot T$	This work
	$L^1(Pb^{2+})_P(MoO_4^{2-},O^{2-})_Q = \mathbf{+46250}$	This work
	$L^0(Pb^{2+})_P(MoO_4^{2-},MoO_3)_Q = \mathbf{+147825–151} \cdot T$	This work
	$L^1(Pb^{2+})_P(MoO_4^{2-},MoO_3)_Q = \mathbf{+126960–75.5} \cdot T$	This work
Hexavalent molybdates	$G_{PbMoO_4} = -1092267.81 + 614.510765 \cdot T - 112.192229 \cdot T \cdot \ln(T) - 0.032775 \cdot T^2 + 482846.944 \cdot T^{-1} + 3.86243333 \cdot 10^{-6} T^3$	This work
	$G_{Pb_2MoO_5} = -1334786 + 920.31 \cdot T - 169.2 \cdot T \cdot \ln(T) - 0.033345 \cdot T^2 + 995000 \cdot T^{-1}$	This work
	$G_{Pb_5MoO_8} = G_{Pb_2MoO_5} + 3 * G_{PbO} - \mathbf{4380}$	This work

Table 7
Optimised standard enthalpies of formation and standard entropies of the ternary lead molybdates.

Compound	$\Delta_f H^{\circ}_m$(298.15 K) (kJ · mol^{-1})		S°_m(298.15 K) (J · K^{-1} · mol^{-1})	
	Optimised	Selected*	Optimised	Selected*
$PbMoO_4$	− 1052.9	− (1052.9 ± 0.5)	160.9	160.9
Pb_2MoO_5	− 1274.7	− (1274.7 ± 2.3)	244	244.8 ± 7.4
Pb_5MoO_8	− 1936.2	n.a.	443	n.a.

*Values selected after literature review, see Section 2.

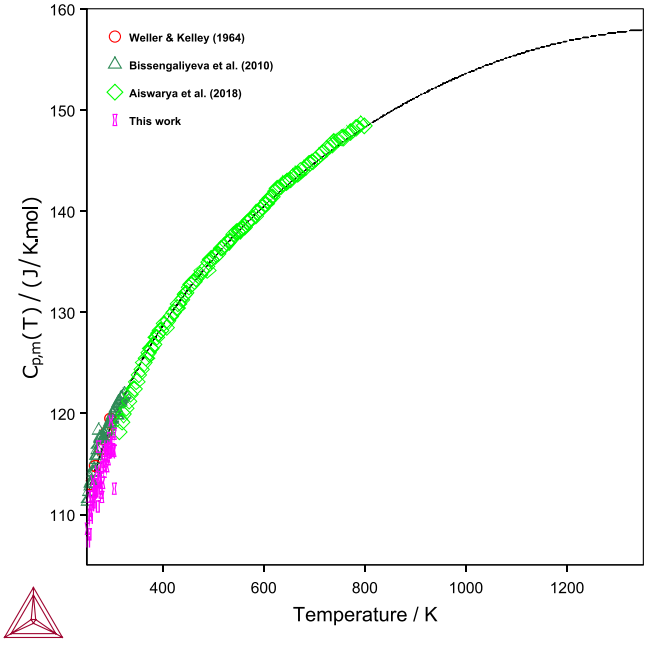

Fig. 8. Heat capacity of $PbMoO_4$ in the model compared with data from refs. [9,66–68].

6.3. Phase diagram data

The calculated PbO-MoO_3 phase diagram is shown in Fig. 11, together with the available phase diagram data. The optimised invariant equilibria are listed in Table 8, together with data from the literature. A

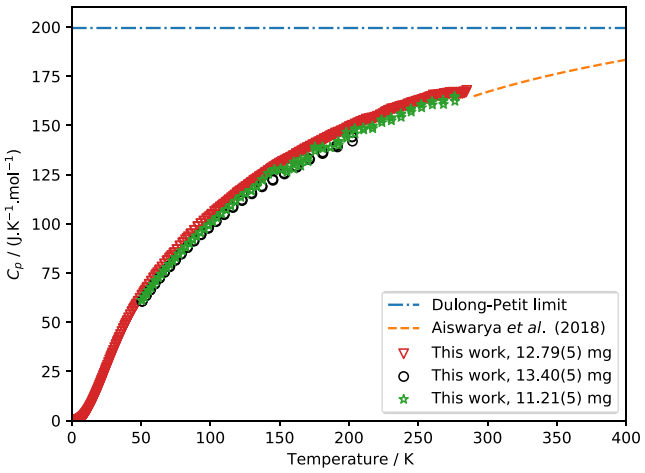

Fig. 9. Low temperature heat capacity of Pb_2MoO_5 as measured in this work and compared to the high-temperature heat capacity as measured by Aiswarya *et al.* [9] and the Dulong-Petit limit.

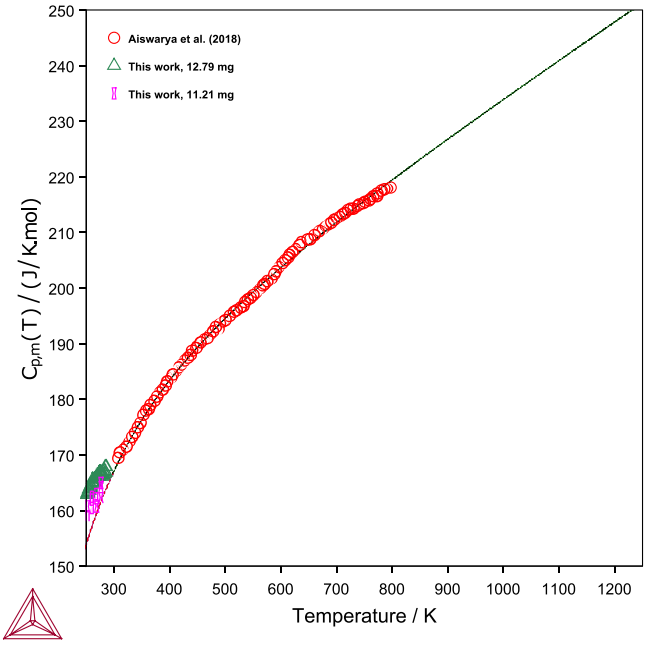

Fig. 10. Heat capacity of Pb_2MoO_5 in the model compared with data from ref. [9].

zoom of the phase diagram around the peritectic decomposition of Pb_5MoO_8 is shown in Fig. 12. The model has been optimised to the data of Kunev *et al.* [73], Bukhalova *et al.* [74] and Nihtianova *et al.* [76] (filled data points).

This equilibrium phase diagram cannot easily be compared to the phase diagram reported by Eissa *et al.* [75] (which is not included in the Figure), because PbO_2 was used as starting material in their study. The compounds Pb_2MoO_5 and $PbMoO_4$ in that phase diagram are more unstable than calculated here, likely because of the stability of Pb(IV) at the oxygen potentials in their work. Their findings for the liquidus are in line with the current modelled phase fields, except at the PbO-rich side of the phase diagram.

Ternary isotherms at 298, 773, 998 and 1273 K are calculated and shown in Fig. 13. There are quite some phase field investigations reported in literature. In the field PbO-MoO_3-O, the change in stable species results from the changes in the PbO-O phase diagram; no ternary compounds with Pb(IV) are stable. In the fields between PbO-MoO_3-

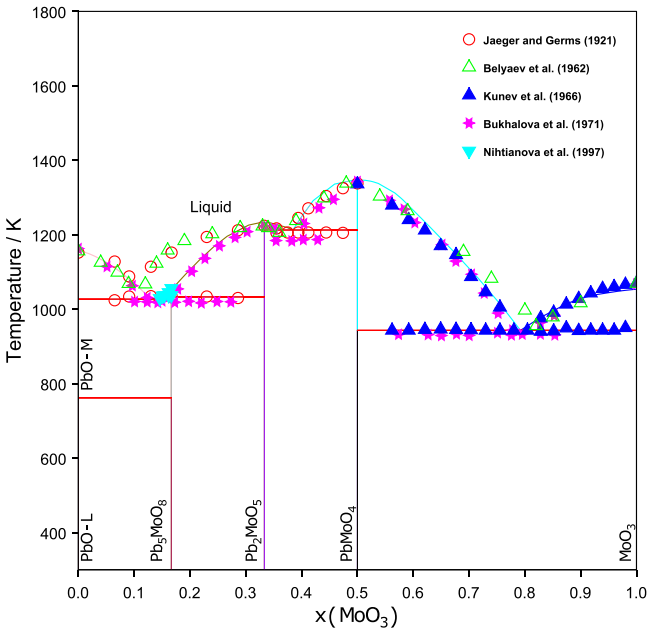

Fig. 11. Pseudo-binary phase diagram PbO-MoO_3 calculated from the optimised thermodynamic model and compared with literature.[7,58,72–74].

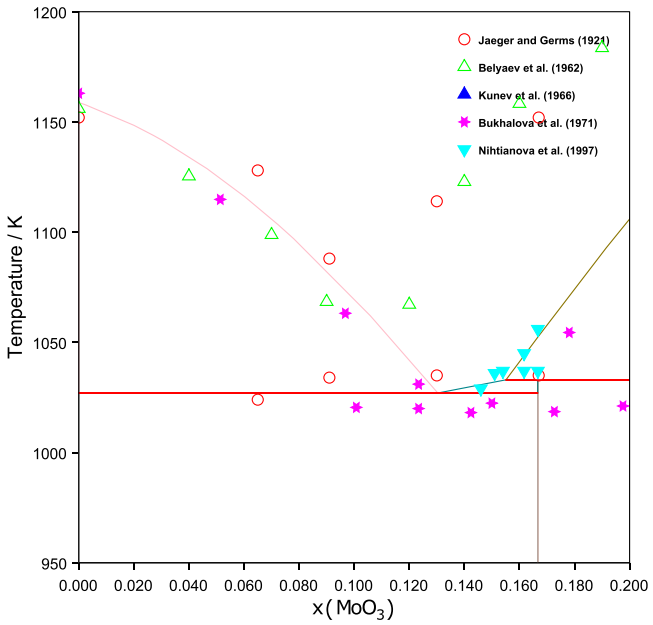

Fig. 12. Pseudo-binary phase diagram PbO-MoO_3, zoomed around the decomposition of Pb_5MoO_8 as calculated from the optimised thermodynamic model and compared with literature.[7,58,72–74].

Table 8
Invariant points on the section PbO-MoO_3; Opt. = optimised in this work. Exp. = experimental.

Invariant equilibrium	Eq. type	x (MoO_3)	T / K	Ref.
PbO + Pb_5MoO_8 = L	Eutectic	0.130	1027	This work, opt.
		0.117	1035	[72]
		0.14	1017	[74]
Pb_5MoO_8 = Pb_2MoO_5 + L	Peritectic decomposition	0.167	1033	This work, opt.
		0.167	1037	[76]
Pb_2MoO_5 = L	Congruent melting	0.333	1232	This work, opt.
		0.333	1224	[7]
		0.333	1225	[72]
		0.333	1223	[74]
		0.333	1223	[76]
Pb_2MoO_5 + $PbMoO_4$ = L	Eutectic	0.38	1212	This work, opt.
		0.375	1208	[72]
		0.375	1183	[74]
$PbMoO_4$ = L	Congruent melting	0.5	1346	This work, opt.
		0.5	1338 ± 2	This work, exp.
$PbMoO_4$ + MoO_3 = L	Eutectic	0.79	943	This work, opt.
		0.825	953	[72]
		0.795	933	[74]
		0.785	945	[73]

MoO_2-Pb at 773 K, the findings of Feja [54] and Aiswarya et al. [8] are in agreement with the current model. Feja also reported the presence of Pb_3O_4 at 773 K above the line PbO-MoO_3. The phase fields as analysed by Aiswarya et al. [8] were measured after cooling to ambient temperature. In their dozens of samples in the field Pb-Mo-O-MoO_3-PbO, they only reported Pb, Mo, MoO_2, $PbMoO_4$, Pb_2MoO_5 and PbO as formed at 773 K, while at 998 K they also found Pb_5MoO_8. As stated above, there remains some contradiction as to the existence of the couple $Pb_3Mo_{16}O_{24}$-$PbMo_5O_8$, that would fall in the Pb-MoO_2-Mo system and thus not influence the chemistry of the remaining fields that are definitely found to be stable.

7. Summary and recommendations

A Pb-Mo-O phase diagram featuring the hexavalent molybdates $PbMoO_4$, Pb_2MoO_5 and Pb_5MoO_8 has been optimised to experimental thermodynamic data using the CALPHAD method. Moreover, the thermal expansion and low temperature heat capacity of the compounds $PbMoO_4$ and Pb_2MoO_5 were measured and the melting enthalpy of $PbMoO_4$ was determined. XANES measurements confirmed the hexavalent oxidation state of Mo of these compounds. The thermodynamic model published in this article includes the phases $PbMoO_4$, Pb_2MoO_5 and Pb_5MoO_8. A model that is consistent with available thermodynamic and phase diagram data was built.

Some recommendations for further experimental work include:

- Measurement of thermodynamic properties (enthalpy of formation, entropy, heat capacity) of Pb_5MoO_8 in order to improve the description of the peritectic decomposition;
- Melting enthalpy of Pb_2MoO_5;
- In-depth structural study of the pair $Pb_3Mo_{16}O_{24}$-$PbMo_5O_8$, to be completed with thermodynamic study to resolve whether these are thermodynamically stable phases that should be considered in the phase diagram;
- Vapour pressure studies to clarify the role of ternary gaseous species.

CRediT authorship contribution statement

Sebastian Couweleers: Investigation. **Rudy J.M. Konings:** Writing – review & editing, Supervision. **Kathy Dardenne:** Investigation. **Jörg Rothe:** Investigation. **Eric Colineau:** Investigation. **Jean-Christophe Griveau:** Investigation, Formal analysis. **Andries van Hattem:** Writing – review & editing, Writing – original draft, Investigation, Formal analysis, Conceptualization. **Robert Dankelman:** Investigation. **Anna L. Smith:** Writing – review & editing, Supervision, Methodology, Funding acquisition, Conceptualization.

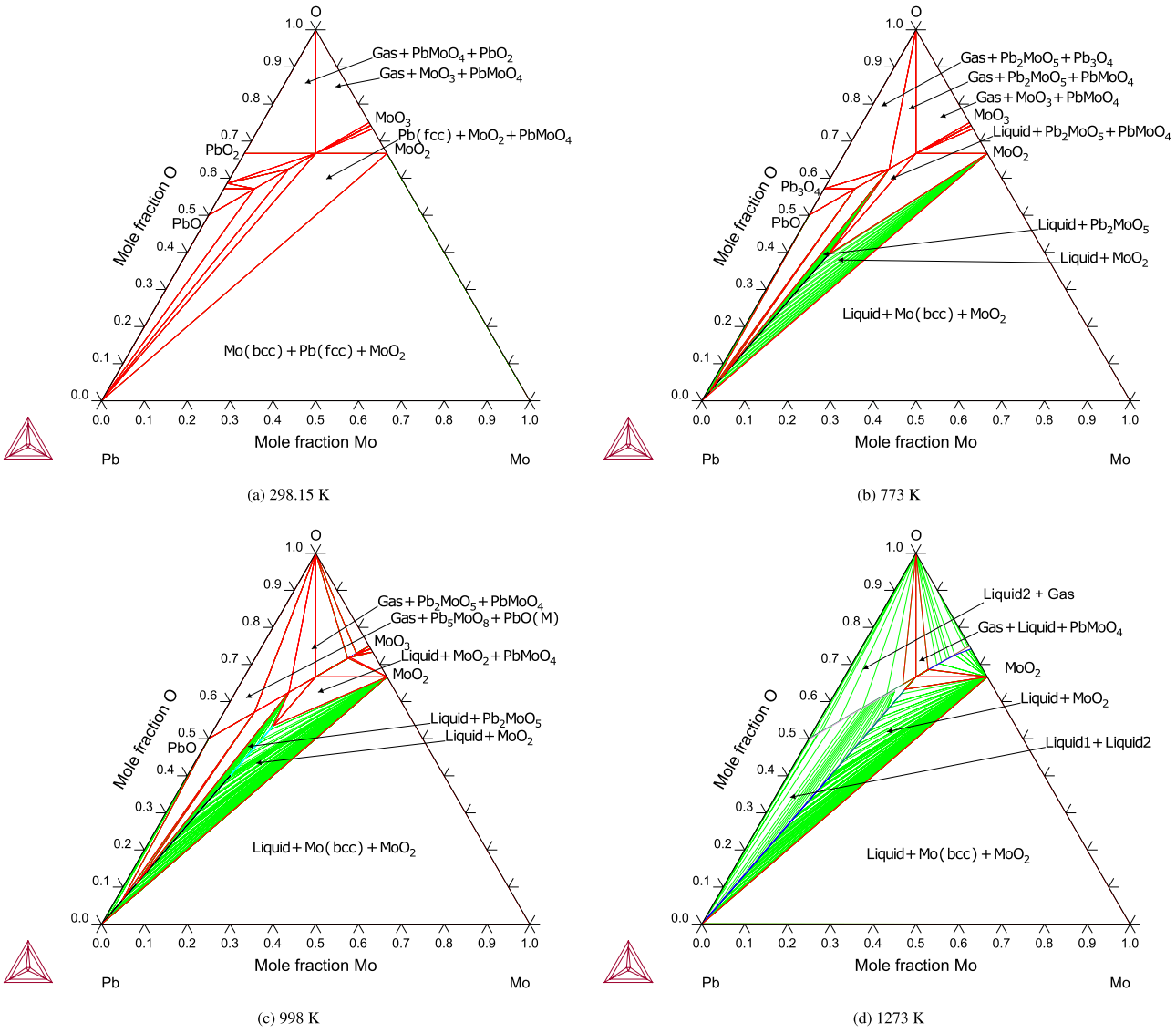

Fig. 13. Calculated isothermal sections of the Pb-Mo-O system at (a) 298.15 K, (b) 773 K, (c) 998 K and (d) 1273 K. The green lines are tie-lines.

Declaration of Competing Interest

The authors declare that they have no known competing financial interests or personal relationships that could have appeared to influence the work reported in this paper.

Data Availability

Data will be made available on request.

Acknowledgements

This work has received funding from the Euratom research and training programme 2019–2020 through the research project PASCAL (Proof of Augmented Safety Conditions in Advanced Liquid-metal-cooled systems) under grant agreement No. 945341.

The Institute for Beam Physics and Technology at KIT is acknowledged for operation of the KARA and the provision of beamtime at the INE-Beamline, operated by the Institute for Nuclear Waste Disposal at the KIT Light Source.

The low temperature heat capacity data reported herein were partially generated through access to the ActUsLab under the Framework for access to the Joint Research Centre Physical Research Infrastructures of the European Commission (PACIFIED-LFR project, Research Infrastructure Access Agreement N^{o} 36345/01).

Appendix A. Supporting information

Supplementary data associated with this article can be found in the online version at doi:10.1016/j.jallcom.2024.175588.

References

[1] F. Danevich, B. Grinyov, S. Henry, M. Kosmyna, H. Kraus, N. Krutyak, V. Kudovbenko, V. Mikhailik, L. Nagornaya, B. Nazarenko, A. Nikolaiko, O. Polischuk, V. Puzikov, A. Shekhovtsov, V. Tretyak, Y. Vostretsov, Feasibility study of $PbWO_4$ and $PbMoO_4$ crystal scintillators for cryogenic rare events experiments, Nuclear Inst. Methods Phys. Res. Sect. A: Acc. Spectr. Detect. Assoc. Equip. 622 (3) (2010) 608–613, https://doi.org/10.1016/j.nima.2010.07.060. ⟨https://www.sciencedirect.com/science/article/pii/S0168900210016748⟩.

[2] W. Van Loo, Luminescence of lead molybdate and lead tungstate. i. experimental, Phys. Status Solidi (A) 27 (2) (1975) 565–574.

[3] W. Van Loo, Luminescence of lead molybdate and lead tungstate. ii. discussion, Phys. Status Solidi (A) 28 (1) (1975) 227–235.

[4] J. Groenink, G. Blasse, Some new observations on the luminescence of $PbMoO_4$ and $PbWO_4$, J. Solid State Chem. 32 (1) (1980) 9–20.

[5] S. Nedilko, V. Chornii, Y. Hizhnyi, M. Trubitsyn, I. Volnyanskaya, Luminescence spectroscopy and electronic structure of the $PbMoO_4$ and Pb_2 MoO_5 single crystals, Opt. Mater. 36 (10) (2014) 1754–1759.
[6] G. Loiacono, J. Balascio, R. Bonner, A. Savage, Crystal growth and characterization of lead molybdate, J. Cryst. Growth 21 (1) (1974) 1–11.
[7] F. Jaeger, H. Germs III, über die binären systeme der sulfate, chromate, molybdate und wolframate des bleies, Z. F. üR. Anorg. und Allg. Chem. 119 (1) (1921) 145–173.
[8] P. Aiswarya, R. Ganesan, T. Gnanasekaran, Partial phase diagrams of Pb-Mo-O system and the standard molar Gibbs energy of formation of $PbMoO_4$ and Pb_2 MoO_5, J. Nucl. Mater. 493 (2017) 310–321.
[9] P. Aiswarya, R. Ganesan, T. Gnanasekaran, The standard molar enthalpies of formation and heat capacities of $PbMoO_4$ (s) and Pb_2 MoO_5 (s), J. Chem. Thermodyn. 116 (2018) 21–31.
[10] J. Weeks, Lead, bismuth, tin, and their alloys as nuclear coolants, Nucl. Eng. Des. 15 (4) (1971) 363–372.
[11] J. Zhang, Lead–bismuth eutectic (LBE): A coolant candidate for gen. IV advanced nuclear reactor concepts, Adv. Eng. Mater. 16 (4) (2014) 349–356.
[12] D. Zverev, S. Neevin, D. Doronkov, L. Sokolova, Nuclear ship reactor installations: from gen 1 to 5, At. Energy 129 (1) (2020) 1–7.
[13] H.A. Abderrahim, P. Kupschus, E. Malambu, P. Benoit, K. Van Tichelen, B. Arien, F. Vermeersch, P. D'hondt, Y. Jongen, S. Ternier, et al., Myrrha: A multipurpose accelerator driven system for research & development, Nuclear Instr. Methods Phys. Res. Sect. A: Accelerators, Spectr. Detect. Assoc. Equip. 463 (3) (2001) 487–494.
[14] H.A. Abderrahim, P. Baeten, D. De Bruyn, R. Fernandez, Myrrha–a multi-purpose fast spectrum research reactor, Energy Convers. Manag. 63 (2012) 4–10.
[15] U. S. DOE Nuclear Energy Research Advisory Committee, Generation IV International Forum, A technology roadmap for generation iv nuclear energy systems, ⟨https://www.gen-4.org/gif/jcms/c_40481/technology-roadmap⟩ (2002).
[16] E. Adamov, A. Kaplienko, V. Orlov, V. Smirnov, A. Lopatkin, V. Lemekhov, A. Moiseev, Brest lead-cooled fast reactor: From concept to technological implementation, At. Energy 129 (4) (2021) 179–187.
[17] C.F. Smith, L. Cinotti, Lead-cooled fast reactor, in: Handbook of Generation IV Nuclear Reactors, Elsevier, 2016, pp. 119–155.
[18] M. Pelletier, Y. Guérin, Fuel performance of fast spectrum oxide fuel, in: R. Konings, R. Stoller (Eds.), Comprehensive Nuclear Materials, 2nd edition, Elsevier, 2020, pp. 72–105. Ch. 2.03.
[19] H. Kleykamp, The chemical state of the fission products in oxide fuels, J. Nucl. Mater. 131 (2-3) (1985) 221–246.
[20] F. Cappia, B.D. Miller, J.A. Aguiar, L. He, D.J. Murray, B.J. Frickey, J.D. Stanek, J. Harp, Electron microscopy characterization of fast reactor mox joint oxyde-gaine (jog), J. Nucl. Mater. 531 (2020) 151964.
[21] S. Imoto, Chemical state of fission products in irradiated UO_2, J. Nucl. Mater. 140 (1) (1986) 19–27.
[22] M. Tourasse, M. Boidron, B. Pasquet, Fission product behaviour in phenix fuel pins at high burnup, J. Nucl. Mater. 188 (1992) 49–57.
[23] A. van Hattem, J. Vlieland, R. Dankelman, M.A. Thijs, G. Wallez, K. Dardenne, J. Rothe, R.J. Konings, A.L. Smith, Structural studies and thermal analysis in the Cs_2 MoO_4-$PbMoO_4$ system with elucidation of β-Cs_2 $Pb(MoO_4)_2$, Inorg. Chem. 62 (18) (2023) 6981–6992.
[24] A.K. Rivai, M. Takahashi, Compatibility of surface-coated steels, refractory metals and ceramics to high temperature lead–bismuth eutectic, Prog. Nucl. Energy 50 (2-6) (2008) 560–566.
[25] E. Serag, B. Caers, P. Schuurmans, S. Lucas, E. Haye, Challenges and coating solutions for wear and corrosion inside lead bismuth eutectic: a review, Surf. Coat. Technol. (2022) 128542.
[26] W. Cairang, S. Ma, X. Gong, Y. Zeng, H. Yang, D. Xue, Y. Qin, X. Ding, J. Sun, Oxidation mechanism of refractory molybdenum exposed to oxygen-saturated lead-bismuth eutectic at 600°C, Corros. Sci. 179 (2021) 109132.
[27] D. Risold, J.-I. Nagata, R. Suzuki, Thermodynamic description of the Pb-O system, J. phase equilibria 19 (3) (1998) 213–233.
[28] C. Gueneau, N. Dupin, L. Kjellqvist, E. Geiger, M. Kurata, S. Gosse, E. Corcoran, A. Quaini, R. Hania, A.L. Smith, et al., TAF-ID: an international thermodynamic database for nuclear fuels applications, Calphad 72 (2021) 102212.
[29] B. Predel, Li-Mg–Nd-Zr, in: B. Predel (Ed.), Phase Equilibria, Crystallographic and Thermodynamic Data of Binary Alloys Volume 5, Springer, 1997, p. 1 (Ch. Mo-Pb).
[30] H. Wriedt, The O-Pb (oxygen-lead) system, J. Phase Equilibria 9 (2) (1988) 106–127.
[31] D. Kobertz, Vaporization and caloric studies on yellow lead oxide PbO, Calphad 65 (2019) 155–164.
[32] O. Knacke, Thermodynamic measurement of lead oxide, Erz. Met. 17 (1964) 28–34.
[33] E. Rodigina, K. Gomel'skii, V. Luginina, Entropy and heat capacity of yellow lead oxide at high temperatures, Russ. J. Phys. Chem. 35 (1961) 884–886.
[34] V. Razzazi, S. Alaei, First-principles calculations of structural and thermodynamic properties of β-PbO, Chin. Phys. B 26 (11) (2017) 116501.
[35] X. Liu, Z. Kang, Y. Shi, H. Liu, Y. Zhang, M. He, Binary and ternary phase diagrams of lead, bismuth, and lead oxide, Fluid Phase Equilibria 559 (2022) 113461.
[36] R. Ganesan, T. Gnanasekaran, R.S. Srinivasa, Standard molar gibbs free energy of formation of PbO (s) over a wide temperature range from emf measurements, J. Nucl. Mater. 320 (3) (2003) 258–264.
[37] R. Ganesan, T. Gnanasekaran, R.S. Srinivasa, Diffusivity, activity and solubility of oxygen in liquid lead and lead–bismuth eutectic alloy by electrochemical methods, J. Nucl. Mater. 349 (1-2) (2006) 133–149.
[38] J. Lim, K. Gladinez, A. Marino, K. Rosseel, A. Aerts, Solubility of oxygen and metastable limit for PbO nucleation in liquid Pb, JOM 73 (12) (2021) 4023–4029.
[39] M. Čančarevic, M. Zinkevich, F. Aldinger, Thermodynamic assessment of the ternary Cu-Pb-O system, Int. J. Mater. Res. 96 (8) (2005) 879–887.
[40] OECD-NEA, Handbook on lead-bismuth eutectic alloy and lead properties, materials compatibility, thermalhydraulics and technologies, Organisation for Economic Co-Operation and Development, 2015.
[41] E. Corcoran, J.-L. Flèche, N. Dupin, B. Sundman, C. Guéneau, Thermodynamic investigations of the uranium-molybdenum-oxygen system by a coupling of density functional theory and calphad methodologies, Calphad 63 (2018) 196–211.
[42] G. Kauric, Etude de l'interaction entre le combustible mox et le sodium pour la sureté des réacteurs à neutrons rapides à caloporteur sodium (rnr), Study of the Nuclear Fuel-Sodium Coolant Interaction for the Safety Assessment of Sodium-Cooled Fast Reactors (Ph. D. thesis), University Paris-Saclay, France(2020).
[43] A. Smith, M. Rutten, L. Herrmann, E. Epifano, R. Konings, E. Colineau, J.-C. Griveau, C. Guéneau, N. Dupin, Experimental studies and thermodynamic assessment of the Ba-Mo-O system by the calphad method, J. Eur. Ceram. Soc. 41 (6) (2021) 3664–3686.
[44] A.T. Dinsdale, SGTE data for pure elements, Calphad 15 (4) (1991) 317–425.
[45] T. Alden, D. Stevenson, J. Wulff, Solubility of nickel and chromium in molten lead, Trans. Met. Soc. AIME 212 (1958).
[46] L. Brewer, Atomic energy review: Special issue no. 7. molybdenum: physico-chemical properties of its compounds and alloys, Int. At. Energy Auth. (1980) 714.
[47] B.M. Thaddeus, Binary alloy phase diagrams second edition, Materials Park Ohio (1990)2705-2708.
[48] V. Volodin, Y. Tuleushev, K. Tsai, E. Zhakanbaev, et al., New Mo_3 Pb phase with A15 structure formed in solid solutions of film molybdenum-lead system, Phys. Met. Metallogr. 115 (5) (2014) 500–506.
[49] S. Petrushenko, S. Dukarov, V. Sukhov, Stability limits of the liquid phase in the layered mo/pb/mo, mo/bi/mo and mo/in/mo film systems, J. Nano- Electron. Phys. 8 (42) (2016) 04073-1.
[50] W. Doyle, F. Forbes, Determination by diffuse reflectance of the stoicheiometry of solid products in solid-solid additive reactions, J. Inorg. Nucl. Chem. 27 (6) (1965) 1271–1280.
[51] R. Dronskowski, A. Simon, W. Mertin, Synthese und kristallstruktur von $PbMo_5O_8$; ein reduziertes oxomolybdat mit $Mo_{10}O_{28}$-oktaederdoppeln, Z. F. üR. Anorg. und Allg. Chem. 602 (1) (1991) 49–63.
[52] S.-L. Wang, J.-Y. Yeh, Pb^{2+} cation ordering in $Pb_3(Mo_4O_6)_4$, Acta Crystallogr. Sect. B: Struct. Sci. 47 (4) (1991) 446–451.
[53] X. Jianxiao, Thermoelectric properties of transition metal oxides and thallium main group chalcogenides, Ph.D. thesis, University of Waterloo (2008).
[54] S. Feja, Darstellung und Charakterisierung ternärer Molybdate in den Systemen M-Mo-O (M = Sn, Pb, Sb), Ph.D. thesis, Technischen Universität Dresden (2004).
[55] H. Takatsu, O. Hernandez, W. Yoshimune, C. Prestipino, T. Yamamoto, C. Tassel, Y. Kobayashi, D. Batuk, Y. Shibata, A.M. Abakumov, et al., Cubic lead perovskite $PbMoO_3$ with anomalous metallic behavior, Phys. Rev. B 95 (15) (2017) 155105.
[56] S.V. Krivovichev, O. Mentre, O.I. Siidra, M. Colmont, S.K. Filatov, Anion-centered tetrahedra in inorganic compounds, Chem. Rev. 113 (8) (2013) 6459–6535.
[57] V. Gabrielian, L. Fedorova, E. Tkachenko, A. Neiman, N. Nikogosian, Crystal growth and physico-chemical properties of lead molybdate in the homogeneity region, Cryst. Res. Technol. 21 (4) (1986) 439–448.
[58] D. Nihtianova, S. Angelova, L. Djonev, T.S. Zheleva, E. Tsukeva, K. Petrov, Phase inhomogeneity of Pb_2MoO_5 single crystals, J. Cryst. Growth 148 (1-2) (1995) 148–154.
[59] L.G. Sillén, A.-L. Nylander, On the oxygen positions in tungstates and molybdates with the scheelite structure, Ark. Kemi Mineral. Geol. 17A (4) (1943) 1–27.
[60] V.V. Atuchin, N. Ivannikova, A. Komonov, N. Kuratieva, I. Loshkarev, N. Pervukhina, L. Pokrovsky, V. Shlegel, The low thermal gradient czochralski crystal growth and microstructural properties of a Pb_2MoO_5 (20-1) cleaved surface, CrystEngComm 17 (24) (2015) 4512–4516.
[61] P. Vassilev, D. Nihtianova, $Pb_5O_4MoO_4$, Acta Crystallogr. Sect. C: Cryst. Struct. Commun. 54 (8) (1998) 1062–1064.
[62] C. Muldrow Jr, L. Hepler, Heats of precipitation and formation of lead and calcium molybdates, J. Phys. Chem. 62 (8) (1958) 982–984.
[63] I. Dellien, K.G. McCurdy, L.G. Hepler, Enthalpies of formation of lead chromate, lead molybdate, and lead tungstate, and the entropy of aqueous tungstate ion, J. Chem. Thermodyn. 8 (3) (1976) 203–207.
[64] M. Bissengaliyeva, L. Ogorodova, M. Vigasina, L. Mel'chakova, Enthalpy of formation of wulfenite (natural lead molybdate), Russ. J. Phys. Chem. A 87 (2) (2013) 163–165.
[65] D. Wagman, W. Evans, V. Parker, I. Halow, S. Bailey, R. Schumm, BS Technical Note (1969).
[66] W. Weller, K. Kelley, Low temperature heat capacity and entropies at 298.15K of lead molybdate and lead tungstate, U. S. Bur. Mines Rept. Inv. 6357 (5) (1964) 194.
[67] M.R. Bissengaliyeva, M.A. Bespyatov, D.B. Gogol', Experimental measurement and calculation of mole heat capacity and thermodynamic functions of wulfenite $PbMoO_4$, J. Chem. Eng. Data 55 (9) (2010) 2974–2979.
[68] M.R. Bissengaliyeva, D.B. Gogol, N.S. Bekturganov, S.T. Taimassova, M. A. Bespyatov, A.A. Zhusipov, Heat capacity and standard thermodynamic functions of the wulfenite $PbMoO_4$ over the temperature range of (0 to 320) K, J. Chem. Eng. Data 56 (5) (2011) 1941–1945.
[69] L. Glasser, Additive single atom values for thermodynamics I: Volumes, entropies, heat capacities of ionic solids, J. Chem. Thermodyn. 166 (2022) 106685.
[70] E. Nikolaev, K. Ovchinnikov, G. Semenov, On vapor composition over lead molybdate and tungstate, Zh. . Obshchej Khimii 54 (5) (1984) 977–978.

[71] K. Kunkel, E. Milke, M. Binnewies, Formation of ternary lead-molybdenum oxides $PbMoO_4$, $PbMo_2O_7$, Pb_2MoO_5 and $PbMo_3O_{10}$ in the gas phase: A mass spectrometric and quantum chemical investigation, Int. J. Mass Spectrom. 374 (2014) 12–19.
[72] I. Belyaev, N. Smolyaninov, The Bi_2O_3-MoO_3-PbO ternary system, Russ. J. Inorg. Chem. 5 (1962) 579–581.
[73] D. Kunev, L. Belyaevskaya, A. Zelikman, The MoO_3-$CaMoO_4$, MoO_3-$PbMoO_4$ and MoO_3-$ZnMoO_4$ systems, Russ. J. Inorg. Chem. (Engl. Transl.) 11 (1966) 1063–1064.
[74] G. Bukhalova, V. Manakov, V. Maltsev, Equilibrium diagram of the PbO-MoO_3 system, Russ. J. Inorg. Chem. 16 (2) (1971) 280–281.
[75] M. Eissa, M. Elmasry, S. Younis, The PbO_2-Pb-MoO_3 system in air, Thermochim. Acta 288 (1-2) (1996) 169–178.
[76] D. Nihtianova, D. Shumov, S. Angelova, Y.B. Dimitriev, L. Petrov, Investigation of Pb_5MoO_8 crystal growth in PbO-MoO_3 system, J. Cryst. Growth 179 (1-2) (1997) 161–167.
[77] S. Suryanarayana, V. Deshpande, X-ray determination of the thermal expansion of lead molybdate, Curr. Sci. 41 (23) (1972) 837–839.
[78] S. Achary, S. Patwe, A. Vishwanath, S. Wajhal, P. Krishna, A. Tyagi, Evolution of crystal structure of $PbMoO_4$ between 5 and 300 K: a low temperature powder neutron diffraction study, Mater. Chem. Phys. 260 (2021) 124111.
[79] J. Argyle, F. Hummel, Dilatometric and x-ray data for lead compounds, II, J. Am. Ceram. Soc. 46 (1) (1963) 10–14.
[80] B. Mentzen, A. Latrach, J. Bouix, A. Hewat, The crystal structures of $PbO.PbXO_4$ (X = S, Cr, Mo) at 5K by neutron powder profile refinement, Mater. Res. Bull. 19 (5) (1984) 549–554.
[81] H.M. Rietveld, A profile refinement method for nuclear and magnetic structures, J. Appl. Crystallogr. 2 (2) (1969) 65–71.
[82] B. van Laar, H. Schenk, The development of powder profile refinement at the Reactor Centre Netherlands at Petten, Acta Crystallogr. Sect. A: Found. Adv. 74 (2) (2018) 88–92.
[83] J. Rodríguez-Carvajal, Recent advances in magnetic structure determination by neutron powder diffraction, Phys. B: Condens. Matter 192 (1-2) (1993) 55–69.
[84] J. Rothe, S. Butorin, K. Dardenne, M. Denecke, B. Kienzler, M. Löble, V. Metz, A. Seibert, M. Steppert, T. Vitova, et al., The INE-beamline for actinide science at ANKA, Rev. Sci. Instrum. 83 (4) (2012) 043105.
[85] B. Ravel, M. Newville, ATHENA, ARTEMIS, HEPHAESTUS: data analysis for X-ray absorption spectroscopy using IFEFFIT, J. Synchrotron Radiat. 12 (4) (2005) 537–541.
[86] A. Smith, T.P. Thi, C. Guéneau, J.-C. Dumas, E. Epifano, W. van Burik, N. Dupin, Thermodynamic modelling assessment of the ternary system Cs-Mo-O, Calphad 75 (2021) 102350.
[87] P. Javorsky`, F. Wastin, E. Colineau, J. Rebizant, P. Boulet, G. Stewart, Low-temperature heat capacity measurements on encapsulated transuranium samples, J. Nucl. Mater. 344 (1-3) (2005) 50–55.
[88] J. Lashley, M. Hundley, A. Migliori, J. Sarrao, P. Pagliuso, T. Darling, M. Jaime, J. Cooley, W. Hults, L. Morales, et al., Critical examination of heat capacity measurements made on a quantum design physical property measurement system, Cryogenics 43 (6) (2003) 369–378.
[89] C.A. Kennedy, M. Stancescu, R.A. Marriott, M.A. White, Recommendations for accurate heat capacity measurements using a quantum design physical property measurement system, Cryogenics 47 (2) (2007) 107–112.
[90] B. Sundman, B. Jansson, J.-O. Andersson, The Thermo-Calc databank system, Calphad 9 (2) (1985) 153–190.
[91] J.-O. Andersson, T. Helander, L. Höglund, P. Shi, B. Sundman, Thermo-Calc & DICTRA, computational tools for materials science, Calphad 26 (2) (2002) 273–312.
[92] M. Hillert, B. Jansson, B. Sundman, J. Ågren, A two-sublattice model for molten solutions with different tendency for ionization, Metall. Trans. A 16 (1985) 261–266.
[93] H. Aritani, T. Tanaka, T. Funabiki, S. Yoshida, M. Kudo, S. Hasegawa, Structure of Mo-Mg binary oxides in oxidized/reduced states studied by x-ray absorption spectroscopy at the Mo K edge and Mg K edge, J. Phys. Chem. 100 (13) (1996) 5440–5446.
[94] A.P. Freitas, R.F. André, C. Poucin, T.K.-C. Le, J. Imbao, B. Lassalle-Kaiser, S. Carenco, Guidelines for the molybdenum oxidation state and geometry from x-ray absorption spectroscopy at the Mo $L_{2,3}$-edges, J. Phys. Chem. C. 125 (32) (2021) 17761–17773.